



FLOODSTAND-deliverable:

**Results of the computational study  
on the pressure losses in openings**

Authors	Michel Visonneau, Patrick Queutey and Emmanuel Guilmineau
Organisation	CNRS
Revision	1.01b
Deliverable No.	D2.4a

Date	8 October 2010
------	----------------



<b>Document identification sheet</b>	
<b>FLOODSTAND</b>	<b>Integrated Flooding Control and Standard for Stability and Crisis Management</b>
FP7-RTD- 218532	
<b>Title:</b> Results of the computational study on the pressure losses in openings	<b>Other report identifications:</b>
<b>Investigating partners:</b> CNRS, CTO	
<b>Authors:</b> Michel Visonneau, Patrick Queutey and Emmanuel Guilmineau	
<b>Reviewed by:</b>	
<input type="checkbox"/> <b>Outline</b> <input type="checkbox"/> <b>Draft</b> <input checked="" type="checkbox"/> <b>Final</b> <b>Version number:</b> 1.01b <b>Revision date:</b> 8 October 2010 <b>Next version due:</b> <b>Number of pages:</b> 23	<input checked="" type="checkbox"/> <b>A deliverable</b> <input type="checkbox"/> <b>Part of a deliverable</b> <input type="checkbox"/> <b>Cover document for a part of a deliverable</b> <input type="checkbox"/> <b>Deliverable cover document</b> <input type="checkbox"/> <b>Other</b> <b>Deliverable number:</b> D2.4a <b>Work Package:</b> WP2 <b>Deliverable due at month:</b> 17
<b>Accessibility:</b> <input checked="" type="checkbox"/> <b>Public</b> <input type="checkbox"/> <b>Restricted</b> <input type="checkbox"/> <b>Confidential (consortium only)</b> <input type="checkbox"/> <b>Internal (accessibility defined for the final version)</b>	<b>Available from:</b> <a href="http://floodstand.tkk.fi">http://floodstand.tkk.fi</a> <b>Distributed to:</b> <b>Discloses when restricted:</b> <b>Comments:</b>
<b>Abstract:</b> The report contains the results of CFD computations to determine the ability of CFD RANSE solvers to improve the numerical prediction of the pressure loss for a typical opening in different flooding conditions. It also provides investigation of full scale effects over a fully submerged two modules cross-duct with girders and stiffeners.	

**Acknowledgements**

The research leading to these results has received funding from the European Union's Seventh Framework Programme (FP7/2007-2013) under grant agreement n° 218532. The financial support is gratefully appreciated.

**Disclaimer**

Neither the European Commission nor any person acting on behalf of the FLOODSTAND Consortium is responsible for the use, which might be made of the following information. The views expressed in this report are those of the authors and do not necessarily reflect those of the European Commission and other members of the FLOODSTAND Consortium.

Copyright © 2010 FP7 FLOODSTAND project consortium

Reproduction is authorised provided the source is acknowledged

CONTENT

1. EXECUTIVE SUMMARY .....	2
2. SIMULATIONS OF THE FLOW THROUGH A SINGLE MANHOLE .....	3
2.1 Objectives.....	3
2.2 Partners and CFD codes involved.....	3
2.3 The manhole opening .....	3
2.4 Computational domains .....	4
2.4.1 CTO .....	5
2.4.2 CNRS.....	6
2.5 Code settings .....	8
2.6 Results .....	9
2.6.1 Axial force history on manhole .....	9
2.6.2 Flow pattern.....	11
2.6.3 Discharge .....	13
2.7 Conclusions .....	14
3. SUBMERGED CROSS-DUCT SIMULATIONS .....	15
3.1 Scale model .....	15
3.2 Computational domain .....	16
3.3 Model scale simulations .....	17
3.4 Full scale simulations .....	19
3.5 Conclusions .....	20
4. REFERENCES .....	20

## 1. EXECUTIVE SUMMARY

*The goal of this study was to use CFD computations to provide a global and simplified flood-simulation tool with unknown coefficients (pressure loss in various openings, for instance). To do so, a first study performed jointly by CTO and CNRS aimed at computing the flow over a man-hole opening with two different RANSE solvers, CTO using the commercial solver Star-CCM+ and CNRS utilizing their in-house solver, ISIS-CFD. This first part of the study was used (i) to design correct boundary conditions making possible the specification of the requested water elevation in front of the manhole opening, (ii) to assess the influence of the Courant number (i.e. time discretization) on the stability and accuracy of the numerical simulations. Convergent conclusions were drawn by the participants and the agreement between the computations and the experiments held at Aalto University (Ref. 1) was very satisfactory to have confidence in a RANSE solver for this class of complex flows.*

*Based on these findings, CNRS performed a complete study of scale effects over a C2 cross-duct consisting in two modules with girders and stiffeners, a test case described in the deliverable D2.3. For this case, a study of scale effects was carried out which establishes the absence of significant scale effects.*

## 2. SIMULATIONS OF THE FLOW THROUGH A SINGLE MANHOLE

### 2.1 Objectives

The objective of the study is to determine the ability of CFD RANSE solvers to improve the numerical prediction of the pressure loss for a typical opening in different flooding conditions. CNRS and CTO performed RANSE simulations of the flow through a single manhole.

### 2.2 Partners and CFD codes involved

CTO uses STAR-CCM+, a general CFD tool developed by CD-Adapco while CNRS uses their in-house flow solver ISIS-CFD (Ref. 2), a part of FINE™/Marine package distributed by NUMECA Int. and dedicated to marine applications. In both codes, air and water phases are solved using the interface capturing methodology. This implies unsteady simulations even if steady state is expected.

### 2.3 The manhole opening

The dimensions of the single manhole opening are given in Figure 1 with illustration of a typical flow as observed experimentally from the full-scale model in Figure 2.

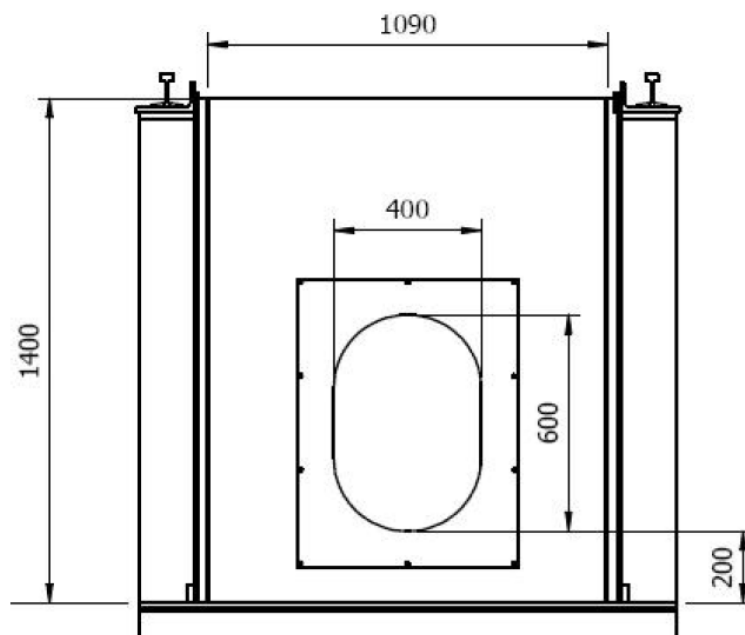


*Figure 1 Dimensions of the manhole*



Figure 2 Flow through single manhole (from AALTO)

Experiments were carried out in a 50m long, 1.09m wide and 1.40m deep flume; see Figure 3 for a schematic overview of the overall system. Different experimental flooding conditions corresponding to a total upstream head ( $H_u$ ) will be considered for comparison with numerical simulations.

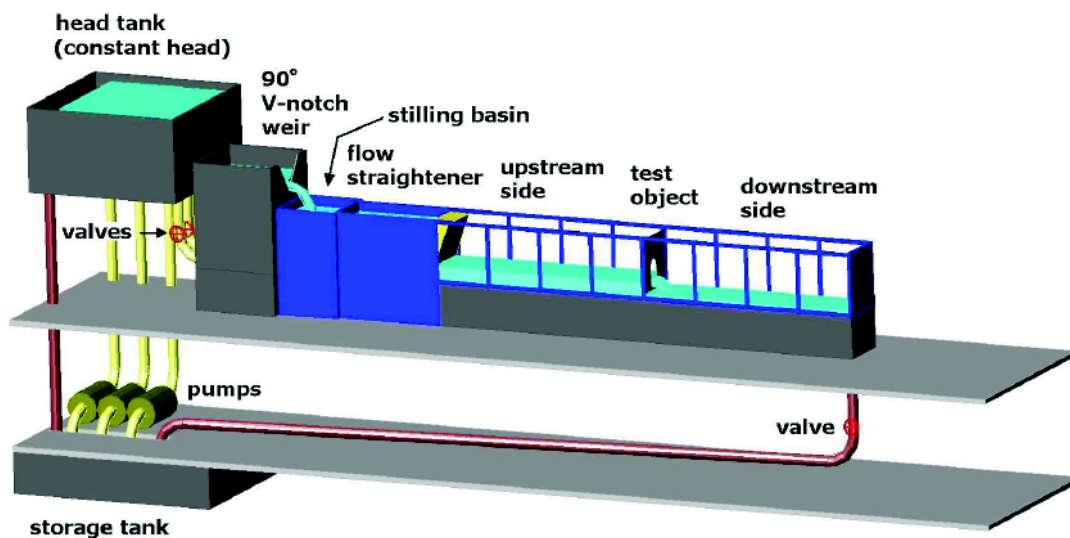


Figure 3 Schematic overview of the experimental system

#### 2.4 Computational domains

Considering the complexity of flume and water circulation system, Fig. 3, CTO and CNRS restricted the computational domain between an inlet section before the test object, and an outlet section located after. The inlet section must be located far upstream enough so that the incoming flow with free-surface is correctly established from the boundary condition used. For the outlet section, it must be located sufficiently downstream of the obstacle. Consequently, no perturbations will influence the flow behaviour in the region of interest around the test object where pressure loss will be computed and compared with measurements. The main numerical difficulty is then to maintain a prescribed water level upstream of the manhole. In this specific study, three different upstream water levels have been considered in agreement with experimental conditions. In any case, the flow is assumed to be symmetric with respect to the Y-symmetry plane, so that only half domain is considered along the principal flow direction.

### 2.4.1 CTO

To overcome the numerical difficulty related to the inlet boundary condition, CTO retained a solution based on prescribed pressure, Figure 4. Previous computations were realized with a prescribed velocity at the inlet; the velocity was uniform and its value was set so as to match the flow discharge resulting from the free flow through the manhole. But no convergence was achieved under that condition, so this method was abandoned.

The computations were performed for the conditions  $H_u=0.15\text{m}$ ,  $0.30\text{m}$   $0.45\text{m}$ , with a downstream water level  $z_d=0.1\text{m}$  for each case, Figure 5. The inlet section is located  $5\text{m}$  upstream of the manhole and the outlet section  $10\text{m}$  downstream.



Figure 4 Initial conditions: zero velocity and hydrostatic pressure

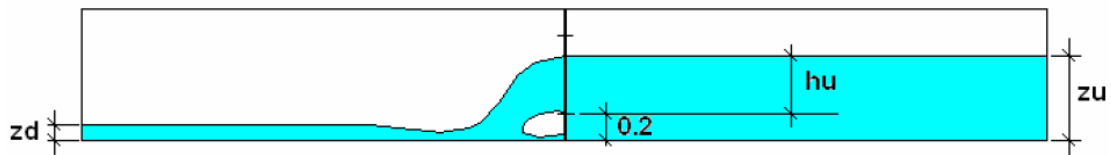


Figure 5 Prescribed water levels

The grid is designed according to the considered water elevation. It is comprised of about  $0.95\text{M}$  cells for the target  $H_u=0.15\text{m}$ ,  $1.35\text{M}$  cells for  $H_u=0.30\text{m}$ , and about  $1.35\text{M}$  cells for  $H_u=0.45\text{m}$ . See Figure 6 to Figure 8 for a detailed view of the mesh around the manhole in the symmetry plane.

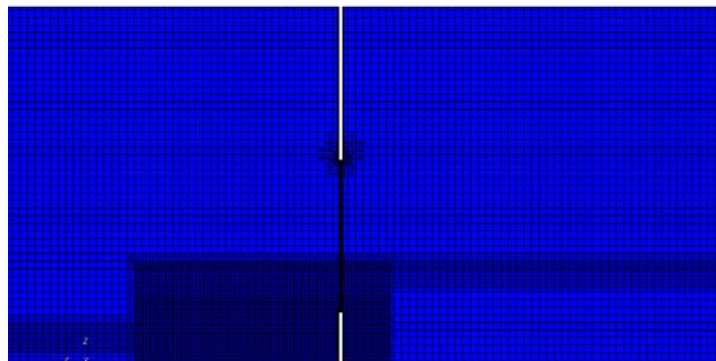
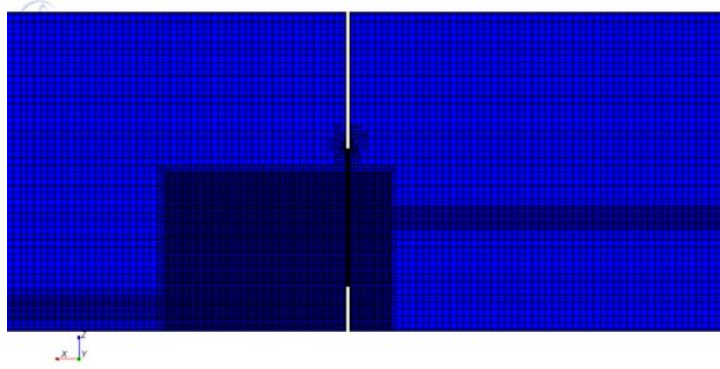
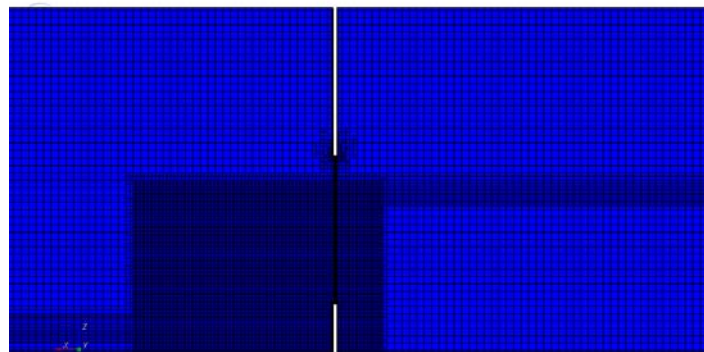


Figure 6 Mesh in symmetry plane:  $H_u=0.15\text{m}$



*Figure 7 Mesh in symmetry plane:  $H_u=0,35m$*



*Figure 8 Mesh in symmetry plane:  $H_u=0,45m$*

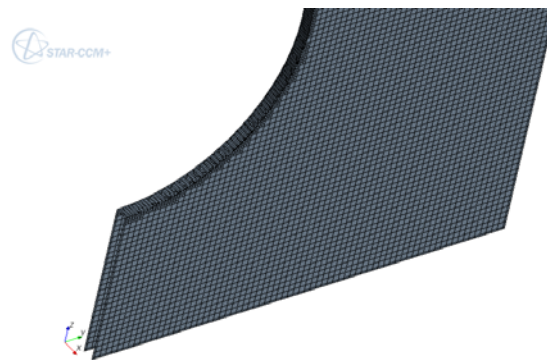


*Figure 9 Mesh at the manhole edges*

The mesh on the manhole and near the edges is shown in Figure 9. The cell sizes are described below:

- Basic size: 30 x 30 x 30 mm,
- Size in the region of the manhole outflow: 7.5 x 7.5 x 7.5 mm,
- Cell height in the free surface region: 7.5 mm.

#### 2.4.2 CNRS

The computational domain with boundary conditions is illustrated with Figure 10. Contrary to the CTO study, initial computations were realized with a prescribed hydrostatic pressure at the inlet and the

assumption of zero pressure gradient at the outlet. Under these circumstances, it was impossible to reach a steady state for the flow in the flume which led us to abandon this approach. The only way to achieve a reliable simulation was to retain the same outlet boundary condition, but to use a prescribed inlet velocity. Consequently, it was necessary to sweep several inlet mass flows to get the correct target water elevation  $H_u$  in front of the manhole. Two grids were used for all the water elevations considered in order to evaluate the discretization errors: a first grid (G0) with about 0,07M points and a second one (G1) with 0,23M points.

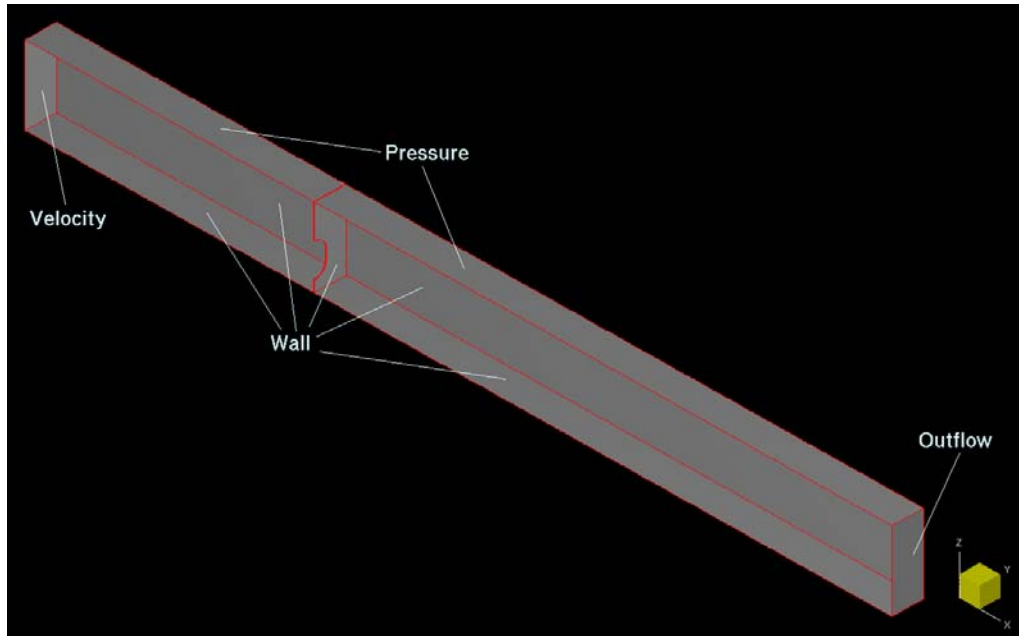


Figure 10 Computational domain and boundary conditions

The G0 mesh is shown in Figure 11 for the symmetry plane only and in Figure 12 for the manhole surface.

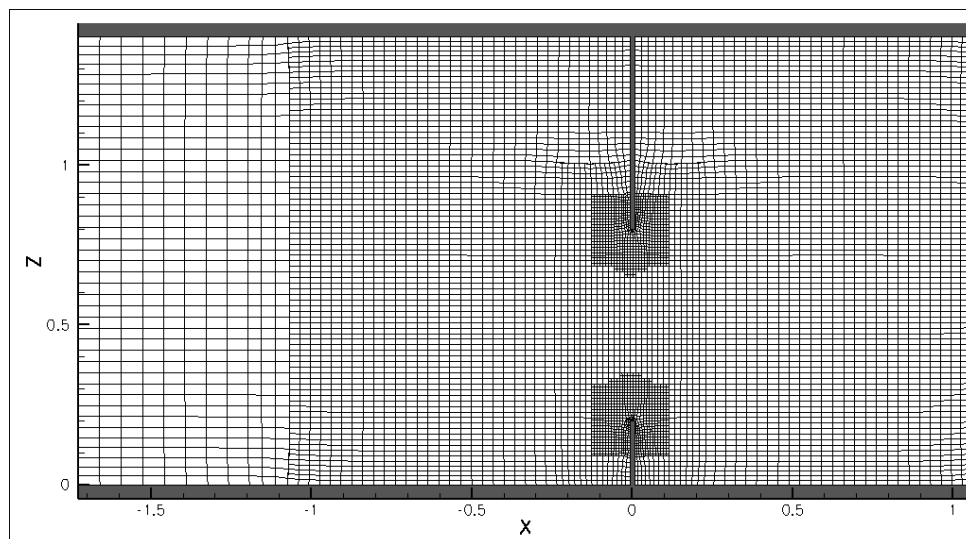


Figure 11 Mesh in symmetry plane (G0 grid).

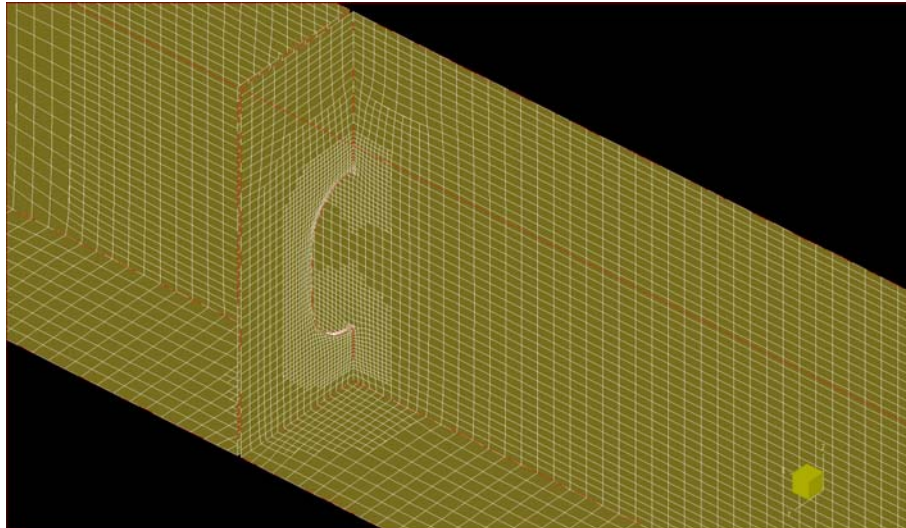


Figure 12 Mesh in symmetry plane and on the manhole (G0 grid)

The mesh cell sizes are summarized in the following table for grids G0 and G1.

Cell sizes: G0 (70,000 cells)	Cell sizes: G1 (223,000 cells)
Inlet region: 70 x 60 x 30 mm	Inlet region: 70 x 60 x 30 mm
Manhole region: 15 - 30 mm (isotropic)	Manhole region: 8.5 - 15 mm (isotropic)
Outflow region: 20 x 10 x 20 cm	Outflow region: 20 x 10 x 20 cm

Table 1 Mesh cell sizes

## 2.5 Code settings

The code settings used by CTO with STAR-CCM+ and CNRS for FINE<sup>TM</sup>/Marine are briefly summarized in the next table:

Parameters	CTO	CNRS
Time step	0.005s	Hu=0.15m : 0.010s Hu=0.20m : 0.005s Hu=0.45m : 0.002s
Number of non-linear iterations per time step	5	8
Under-relaxation factors	Velocity:0.7, Pressure:0.3	Velocity:0.5, Pressure:0.3
Wall boundary conditions	Wall function	Slip

Table 2 Essential code settings

A constant time step was used by CTO independently of the considered case while CNRS time step was adapted to guarantee a Courant number lower than 0.3 for all the cases. Let us notice however that the mean value of 0.005s corresponds to the unique value chosen by CTO. At the vicinity of the free-surface and in the manhole region, the grid density of the CTO grid is comparable to the G1 grid used by CNRS.

## 2.6 Results

### 2.6.1 Axial force history on manhole

It is mandatory for both partners to perform an unsteady simulation even if one is looking for a steady state. Therefore, the time history of the axial force on the manhole in longitudinal direction is a good indicator of the convergence towards a desired steady state. CTO simulations were conducted until  $t=30s$ : Figure 13 to Figure 15 show however that a small oscillation is still present. For CNRS, Fig. 16, it was observed that a steady state was nearly established after 40s. The difference between both partners in terms of convergence to a steady state has to be attributed to different inlet boundary conditions.

With an hydrostatic pressure imposed at the inlet, CNRS observed the same kind of long time oscillations but not damped in time. A reason is that with a prescribed inlet pressure and zero velocity at time  $t=0s$ , CNRS simulations starts with a dam-break like situation near the manhole that generates waves travelling upstream until the inlet, reflecting to the manhole, etc.

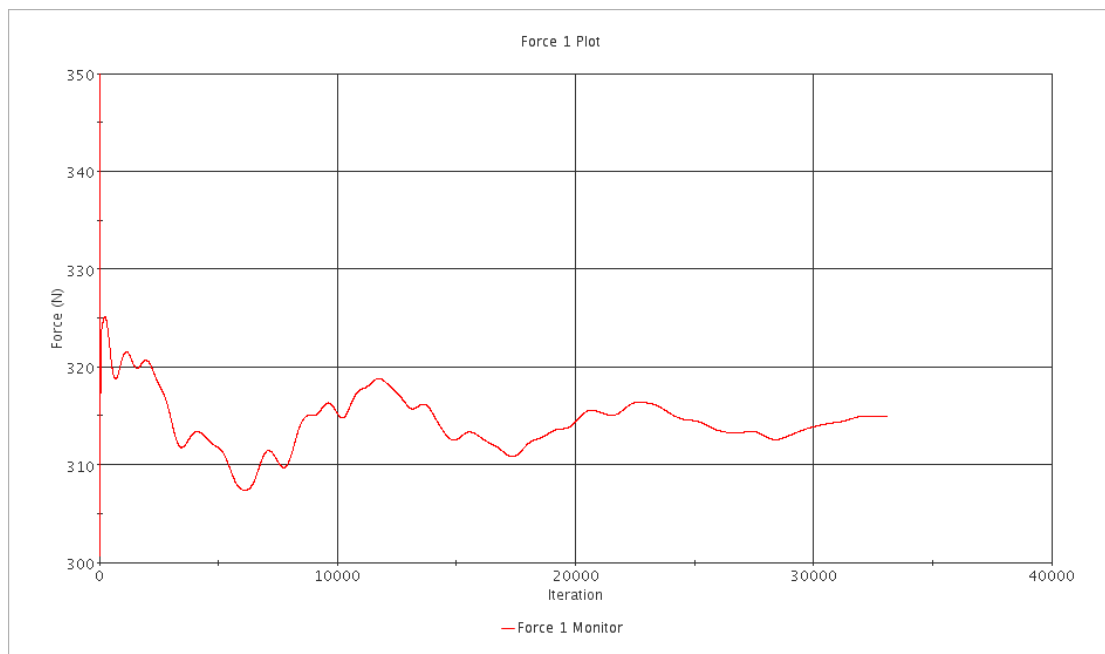


*Figure 13 CTO: axial force history for  $Hu=0.15m$*

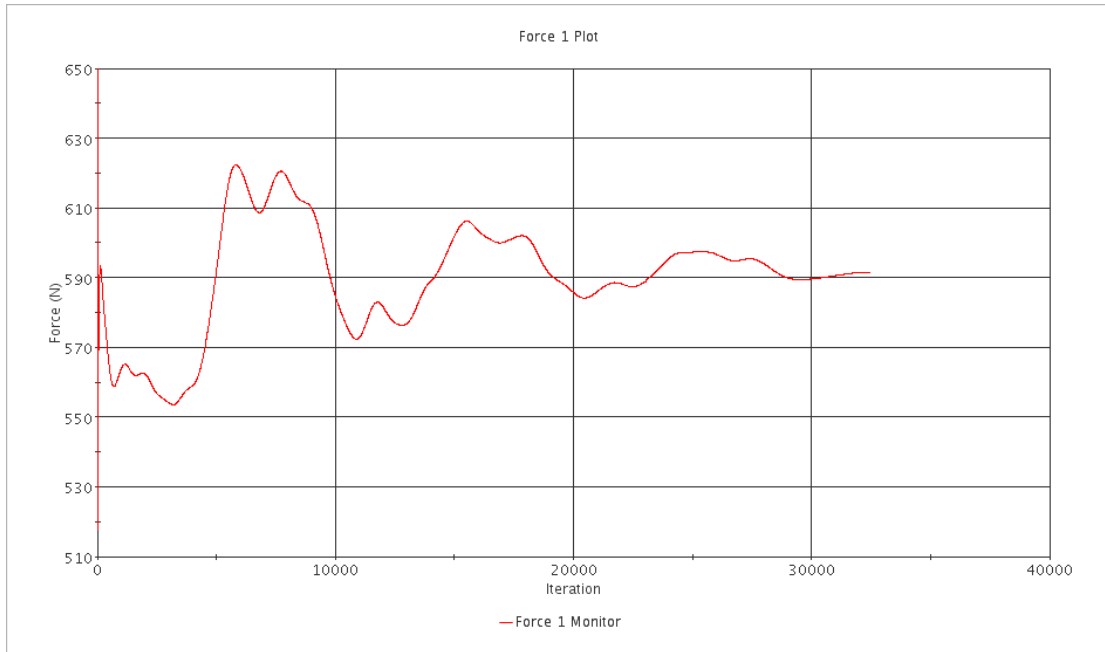


Figure 14 CTO: axial force history for  $Hu=0.30m$

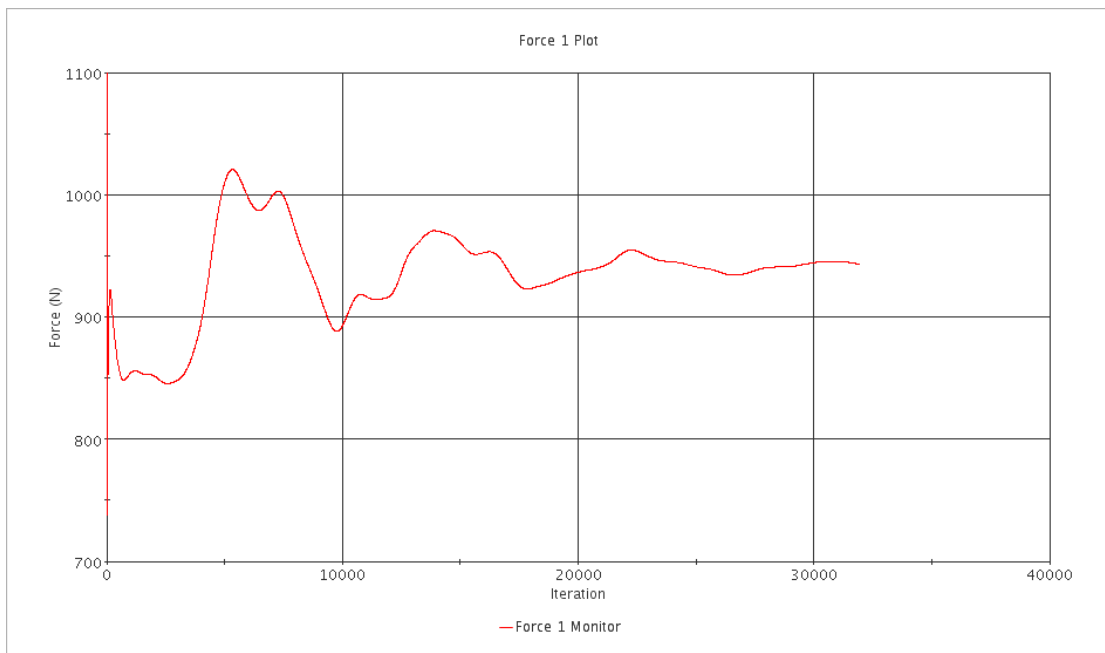


Figure 15 CTO: axial force history for  $Hu=0.45m$

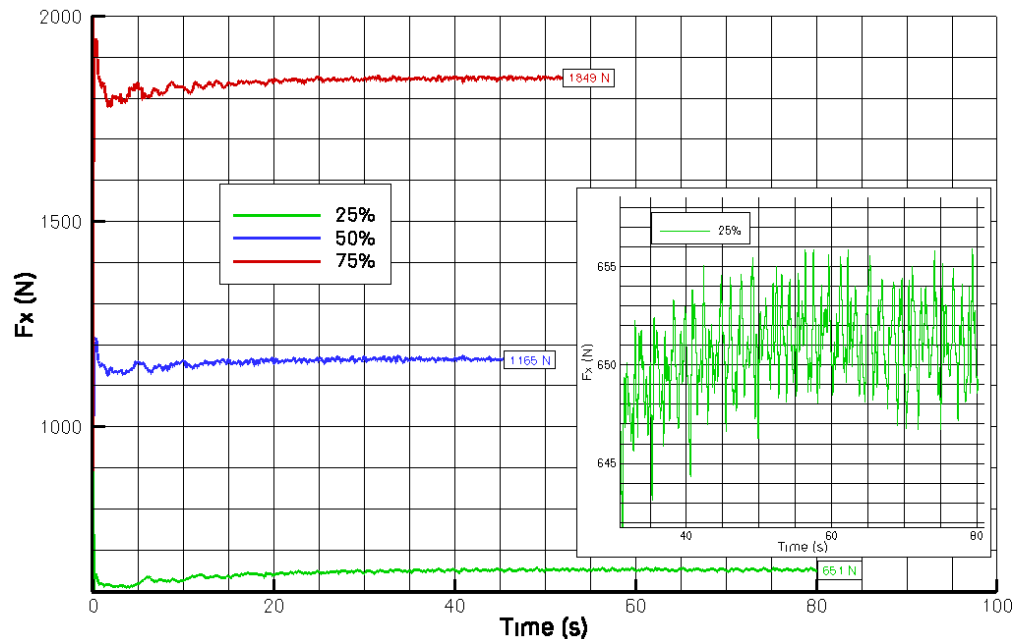


Figure 16 CNRS: axial force histories for  $H_u=0.15m, 0.30,$  and  $0.45m$

If we have a look at Figure 16, right part, we can observe fluctuations in the computed force history after  $t=40s$  for  $H_u=0.15m$  (25% submersion of the manhole). In order to understand the origin of this phenomena, Figure 17 describes the forces exerted by the flow on the upstream (inner) and downstream (outer) surfaces with respect to the manhole. It is then clearly observed that the fluctuations come for the downstream side where the free-surface is not distinguishable due to the presence of a strong and unsteady air-water mixture.

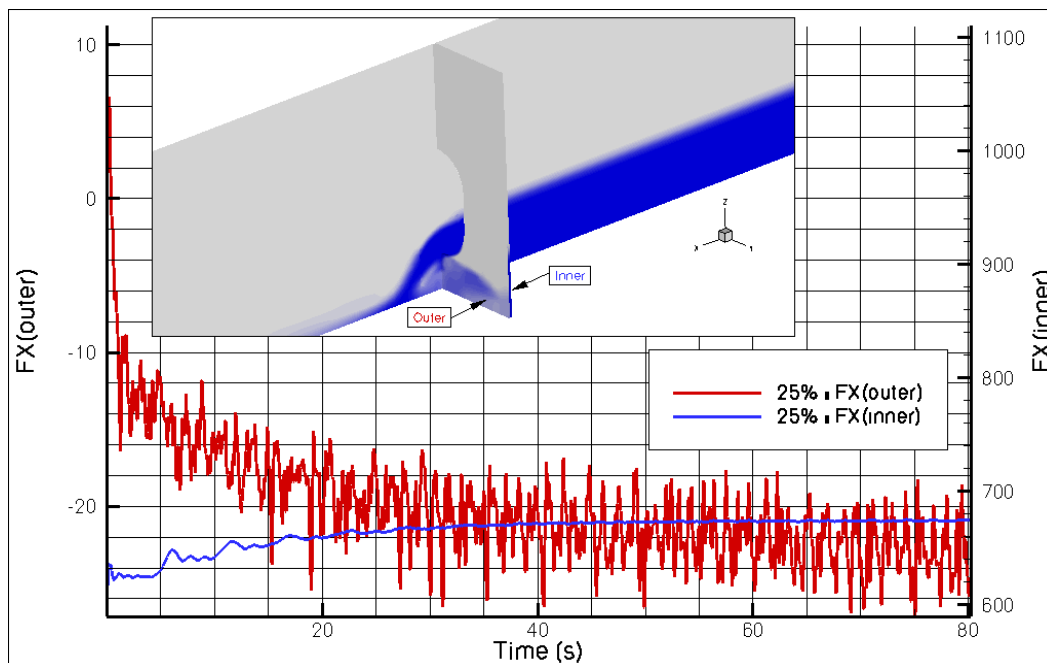


Figure 17 CNRS: axial upstream and downstream force histories for  $H_u=0.15m$

### 2.6.2 Flow pattern

The flow pattern is illustrated with the visualization of the free-surface computed as the iso-surface of the volume fraction 0.5. The experimental target value for the upstream water elevation above the manhole lower edge  $H_u$  is given in the legend of figures (Figure 18 to Figure 20). Table 3 compares the experimental and computed values. Since CTO uses the hydrostatic pressure as inlet boundary

condition, the computed  $H_u$  does not deviate too much from the expected value, the accuracy mainly depending on the vertical grid resolution. On the contrary, the inlet mass-flow prescribed by CNRS does not theoretically guarantee that the target elevation will be reached.

Experimental $H_u$ (target)	CTO computed $H_u$	CNRS computed $H_u$
0.15m	0.151m	0.167m
0.30m	0.301m	0.312m
0.45m	0.444m	0.471m

Table 3 Experimental (target) and computed  $H_u$

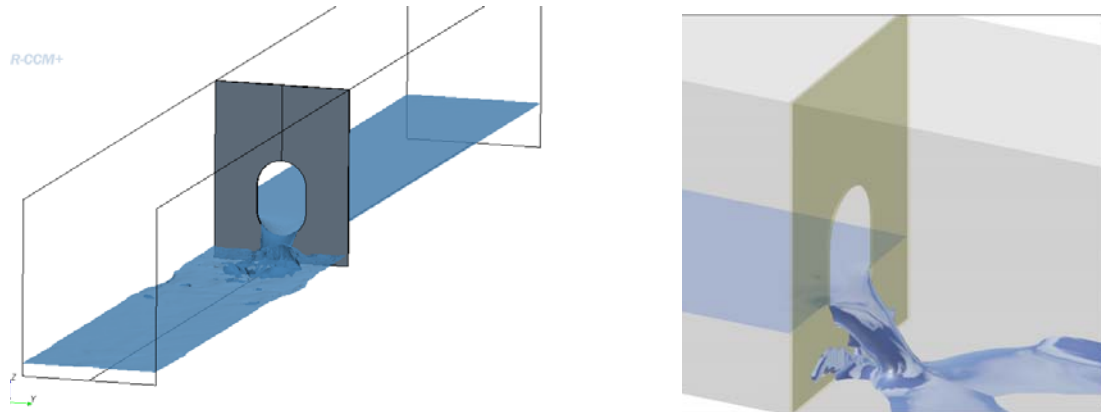


Figure 18 Flow pattern for target  $H_u=0.15m$  (Left: CTO Right: CNRS)

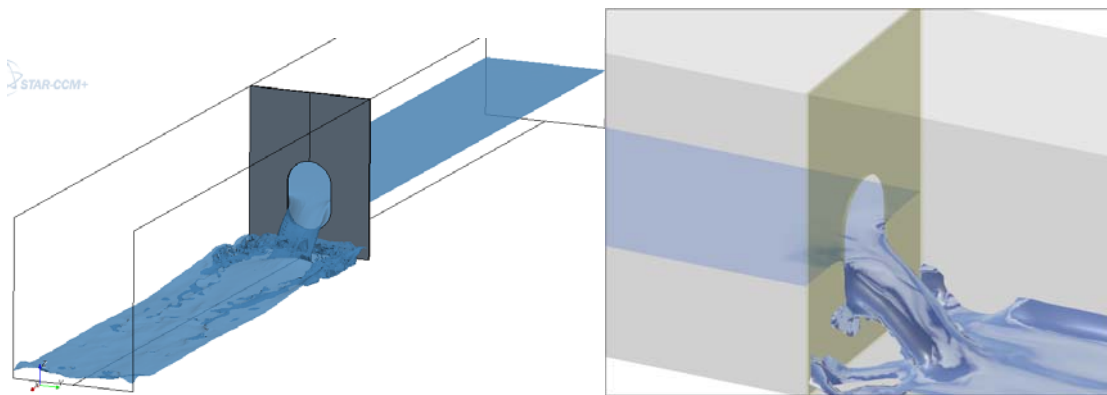


Figure 19 Flow pattern for target  $H_u=0.30m$  (Left: CTO Right: CNRS)

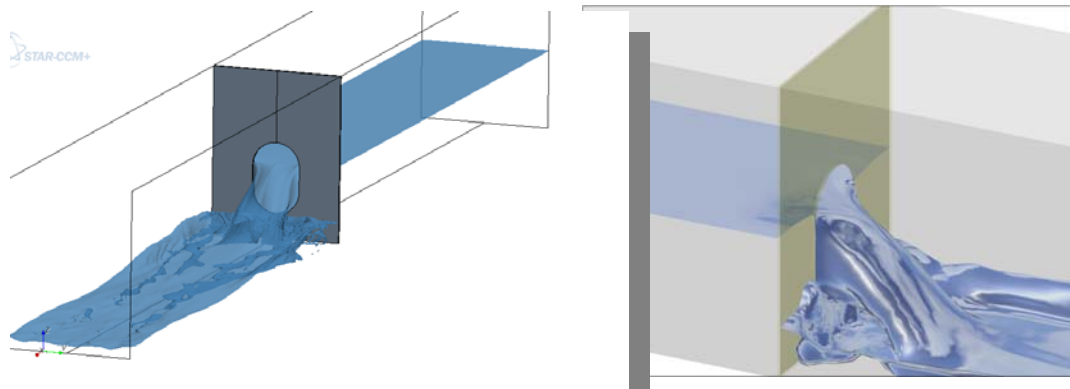


Figure 20 Flow pattern for target  $H_u=0.45m$  (Left: CTO Right: CNRS)

2.6.3 Discharge

The discharge is obtained by integration of the computed flow across the manhole from the axial velocity component  $U_x$  and filtered by the volume fraction ( $C=0$  in air and  $C=1$  in water). Figure 21 for CTO and Figure 22 for CNRS collect the distribution of the filtered  $U_x$  distribution through the manhole using the same colour map for the three water elevations. Except in the vicinity of the manhole region where CTO resolves the wall region while CNRS considers frictionless walls, the shape of the distribution is quite comparable.

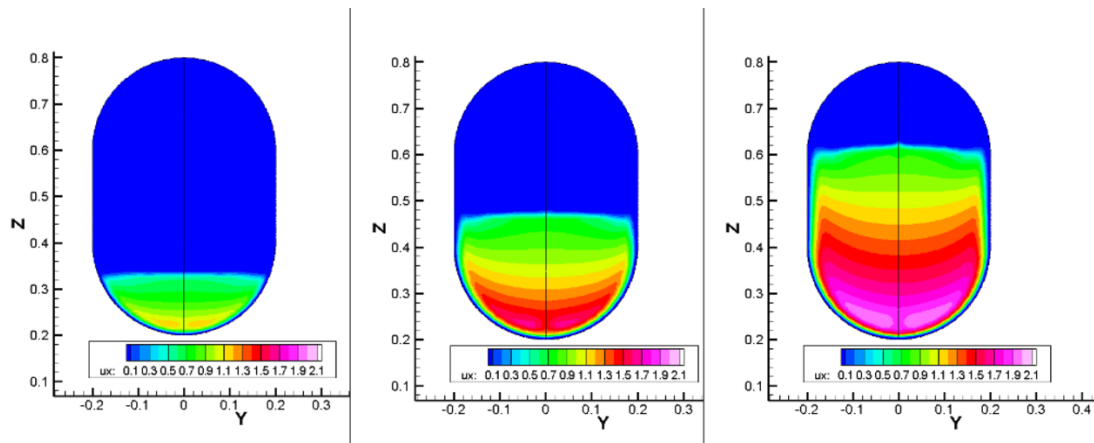


Figure 21 CTO: Volume fraction  $x U_x$  distribution across the manhole

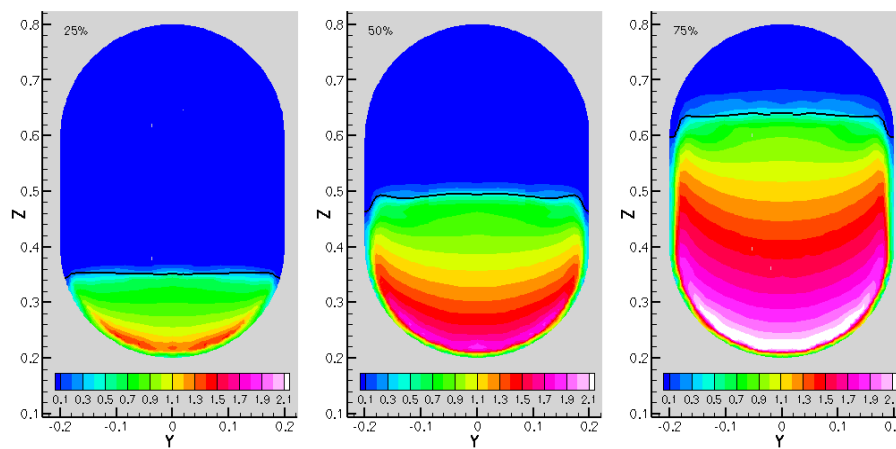


Figure 22 CNRS: Volume fraction  $x U_x$  distribution across the manhole (G1 grid)

In Figure 23, the computed discharge through the manhole has been compared with experiments (“actual discharge” in figure) from Task 2.3I and also from the theoretical approximation (“ideal discharge” in figure).  $H_u$  is the water level above the edge and  $H_o$  the size of the opening (0.6m here).

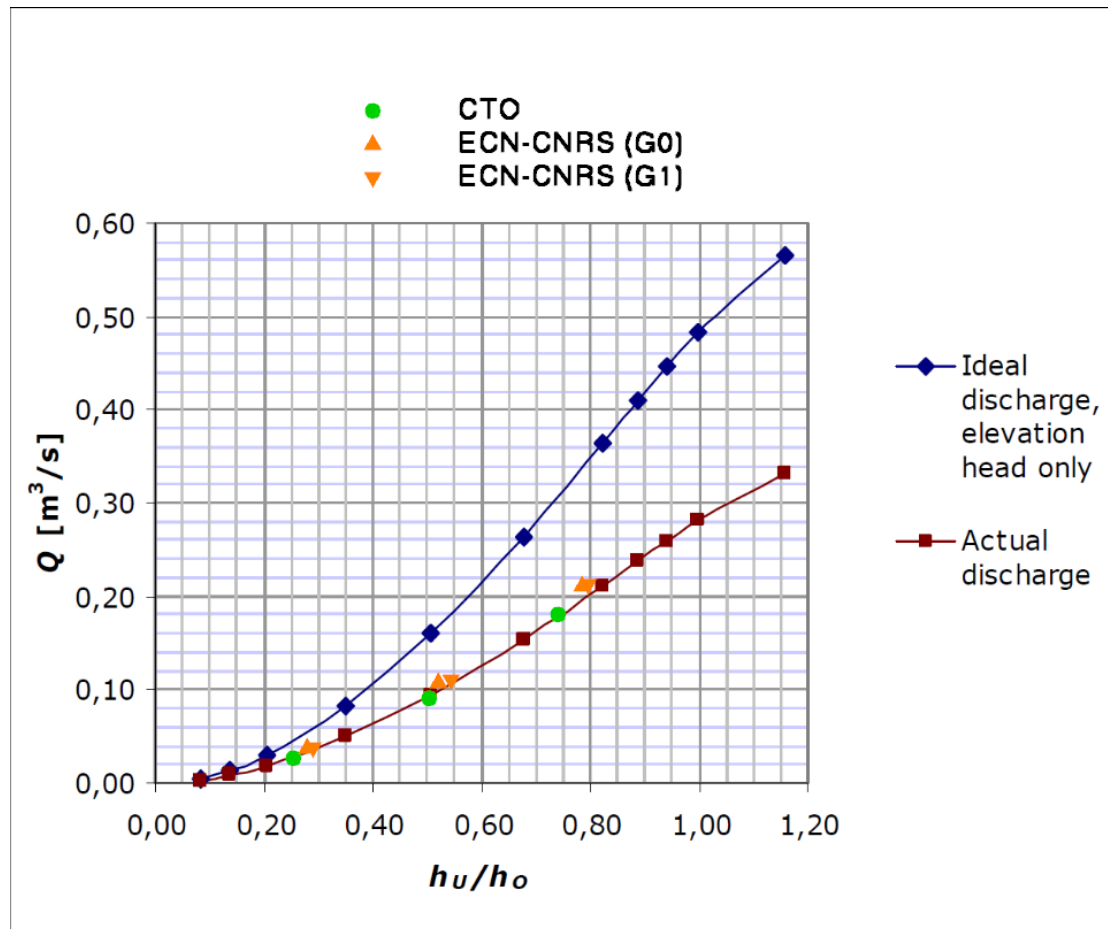


Figure 23 Comparison between experiments (actual discharge), and computations and theory (ideal discharge)

## 2.7 Conclusions

URANSE simulations have been performed to compute the discharge of the flow through a single manhole. Not all the experimental system has been modelled and the computational domain was restricted to the region before and after the manhole. Then, the difficulty was to apply suitable boundary conditions so that various kinds of discharges could be computed and compared with measurements performed by AALTO in Task 2.3I.

CTO first unsuccessfully tried to adapt the inlet velocity during the computation so that a target upstream water elevation could be maintained. Later, they adopted a prescribed hydraulic pressure at the inlet based upon the considered water elevation. However, the convergence to steady state is slow and the flow may be contaminated by travelling waves coming from the initial solution ( $t=0s$ ) similar to a dam-break problem.

CNRS also first tried to use a prescribed inlet pressure from hydrostatic considerations but was not able to damp these travelling waves. Then, they fixed the difficulty by using an inlet velocity distribution based on a prescribed entrance mass flow. This procedure however did not guarantee that the expected water elevation is obtained since it is impossible to impose both the mass flow and the water elevation. This is why, it was necessary to scan various water elevations from various inlet velocities. From this set of first computations, it was possible to compute three targeted water elevations.

Turbulence modelling was taken into account in the CTO simulations with the disadvantage of using grids comprised of up to 1.35M cells. Taking into consideration that the pressure losses at manhole is mainly driven by inviscid effects, CNRS simplified the simulations by considering frictionless walls, which resulted in coarser grids: a first grid G0 having about 70,000 cells and a refined G1 grid in the manhole region with about 230,000 cells. In the region of the manhole and except the walls of the manhole edges, the grid (G1) built by CNRS and CTO have a comparable density with similar code settings.

The flow field distribution in a section across the manhole computed by both partners has been compared. Even if the upstream water elevations are not exactly identical, the shape of the distribution

of the axial velocity used to compute the discharge is comparable. The computed discharge through the manhole has been compared to the measured value for three water levels above the edge and for the same size of the opening. On these three computational points, the comparison is in excellent agreement with the measurements, even for the coarse grid G0 by CNRS. This clearly indicates that a CFD RANSE solver is able to predict the correct discharge, justifying a posteriori the choice made by CNRS in terms of wall boundary conditions.

### 3. SUBMERGED CROSS-DUCT SIMULATIONS

#### 3.1 Scale model

The reference case used for the computational study comes from the experiments documented by Mikael Stening from AALTO, Ref. 2. The C2 cross-duct case was retained that consists in two modules with girders and stiffeners: see Figure 24 and Figure 25.

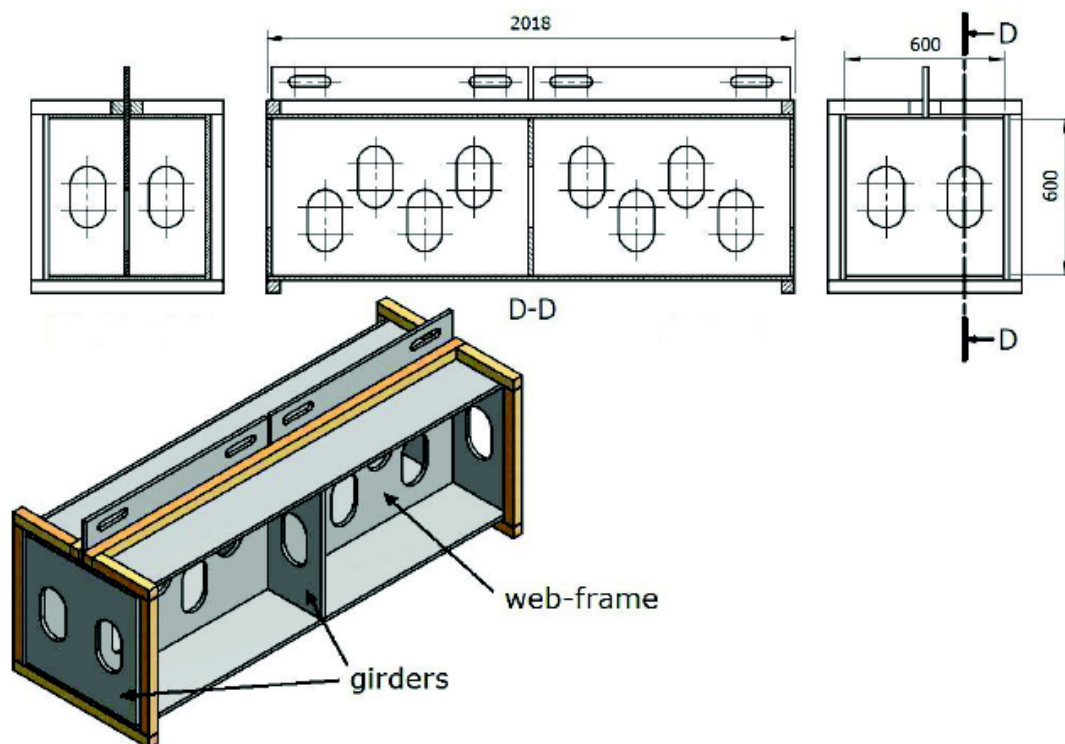


Figure 24 Dimensions of one 1:3 scale model cross-duct module with a web frame in the middle of the cross-duct. The web-frame was not present in the model during most tests.

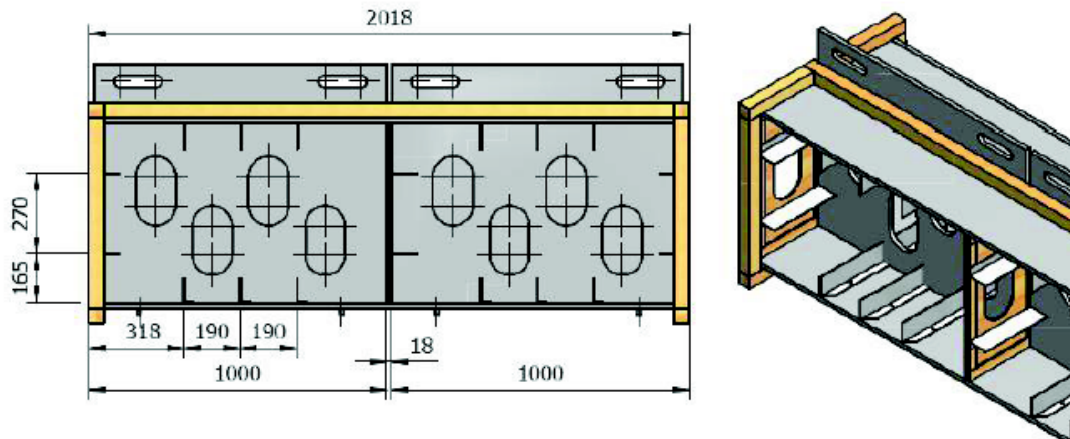


Figure 25 Location of the stiffeners and the web-frame inside a cross-duct module. The stiffeners were located on the girders and the bed and roof of the cross-duct.

### 3.2 Computational domain

The computational geometry is conformed to the experimental one, Figure 26, but restricted to the symmetrical part of the cross-duct where the symmetry plane corresponds to the web-frame plane (green faces). One additional box is added upstream of the module in order to simulate the flow entrance where a water elevation  $h_U$  is prescribed on the top red face with the help of a pressure prescribed boundary condition. In the same way, an additional box is added at the outlet with a prescribed pressure on the blue top face to simulate a prescribed water elevation  $h_D$  for the outflow. All the computations were carried out with the  $k-\omega$  SST turbulence model. Light blue faces correspond to no-slip wall. Everywhere else, wall-function boundary conditions are applied (gray faces).

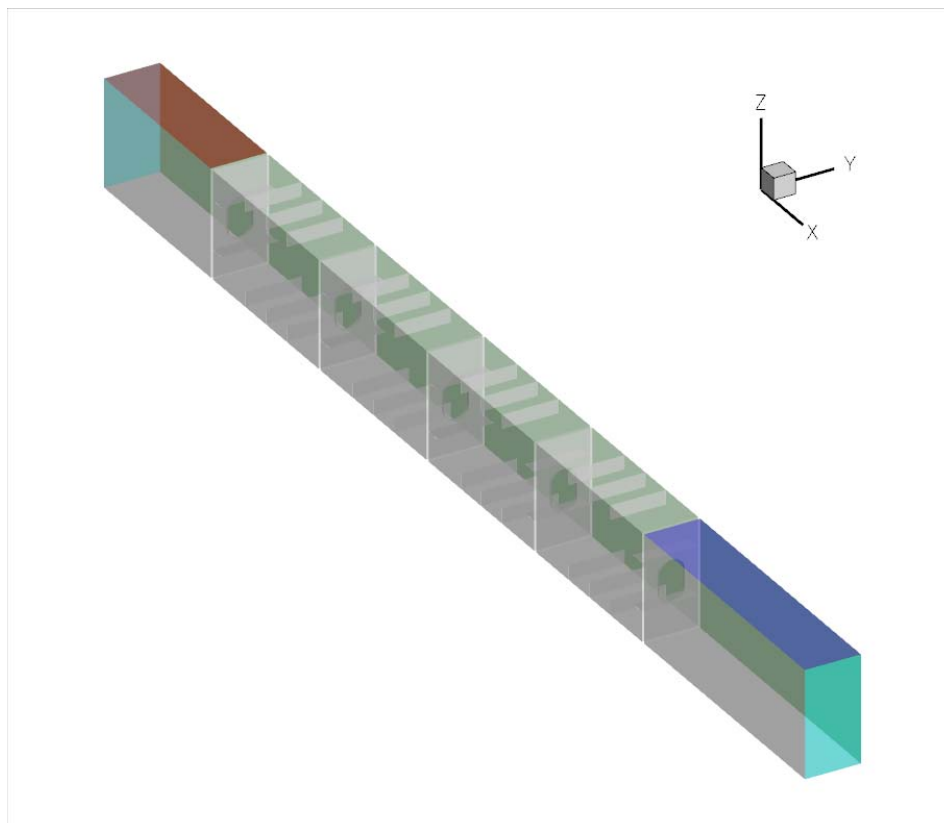


Figure 26 Computational domain of the cross-duct model

The mesh is generated with the automatic HEXPRESS grid generator and contains about 11 million points. Figure 27 illustrates part of the surface grid in the middle region of the cross-duct, and Figure 28 shows the grid density in the same region in a Y-cut.

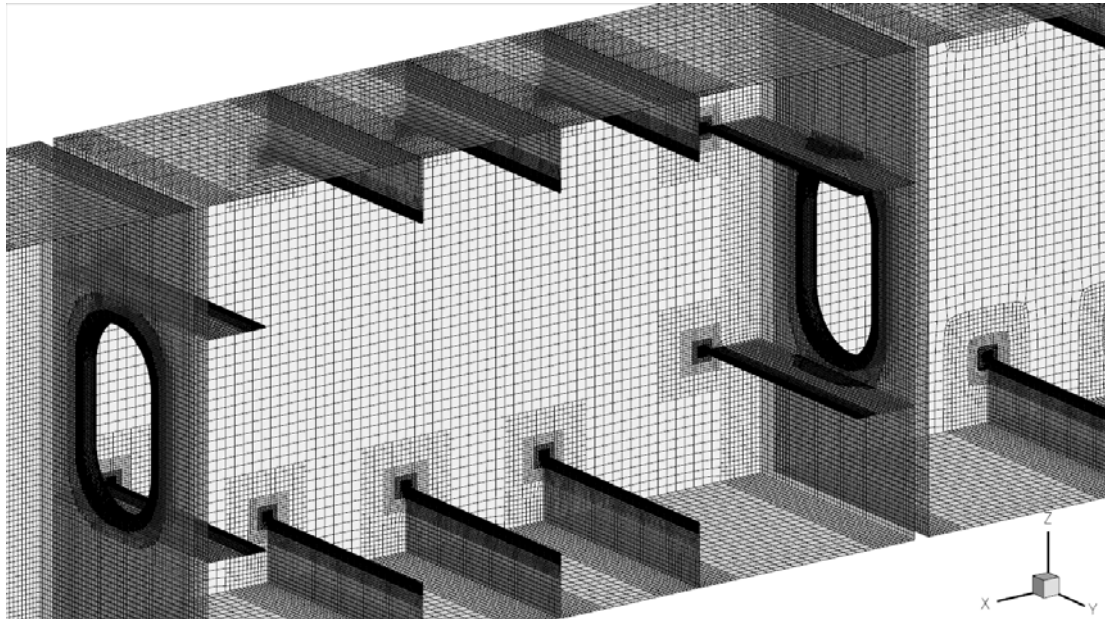


Figure 27 Surface grid details

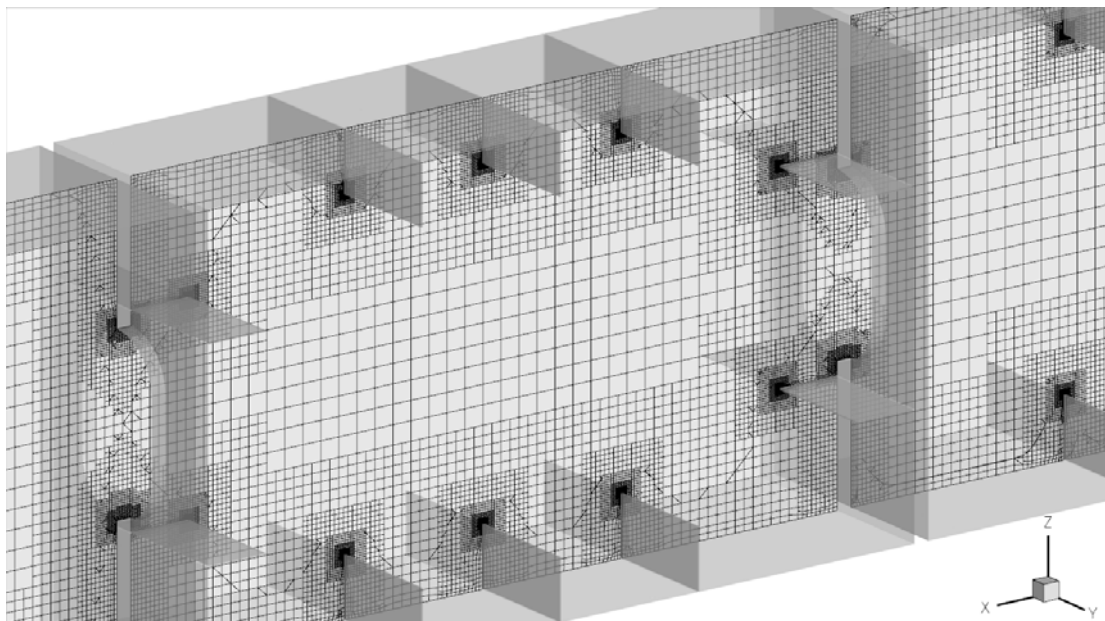


Figure 28 Grid density from a Y-cut

### 3.3 Model scale simulations

A single model scale computation has been performed for a fully immersed cross-duct corresponding to an inlet water height of 1.67m and an output water height of 0.60m corresponding to the cross-duct height. This provides a point located at  $h_D/h_0 = 1.78$  on the abscissa of the discharge coefficient plot (see Fig. 56 in the report about experiments).

Due to code restriction, in order to account for gravity, the computation is performed in an unsteady way starting from fluid at rest with the boundary conditions as mentioned previously. The time step was fixed to 0.001s. Figure 29 represents a Y middle cut of the overall computational domain after  $t=8s$  when the flow is developed. Details showing the presence of the stiffeners are given in Figure 30.

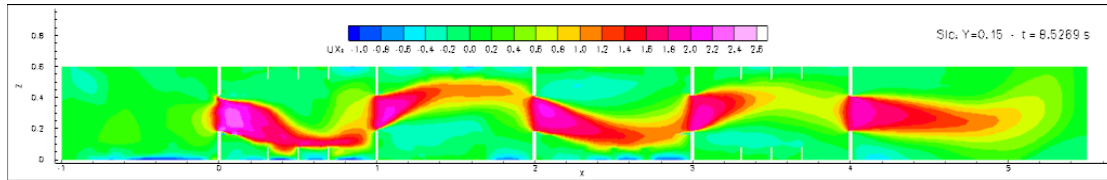


Figure 29 Axial velocity distribution in Y middle cut

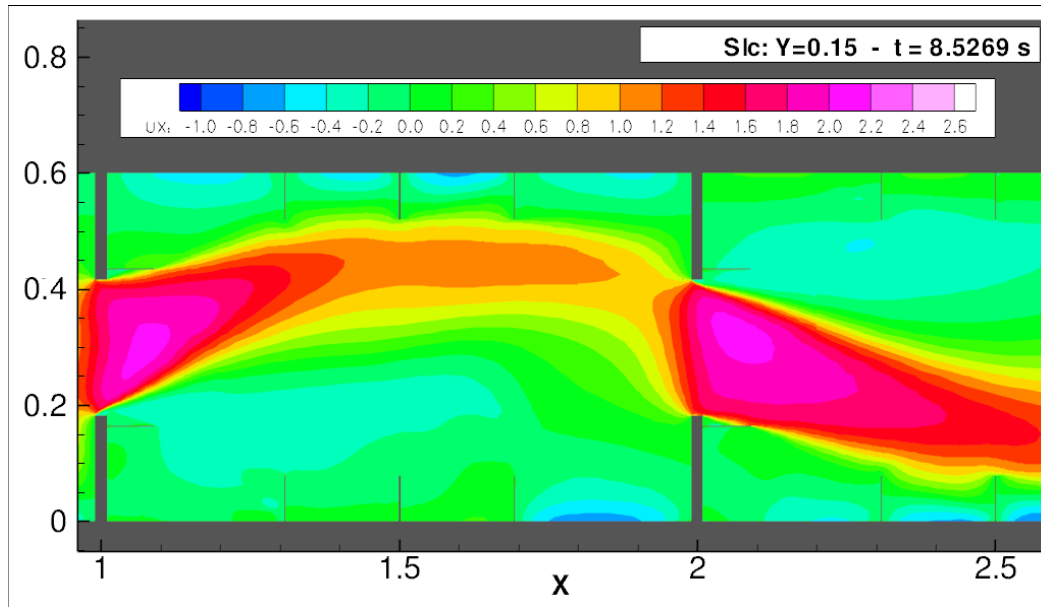


Figure 30 Axial velocity distribution in Y middle cut: details between 1st and 2nd module

The mass flow rate converges to 42 l/s  $\pm$  0.3% and the mass conservation between the first manhole and the fifth manhole is better than 0.1%. The corresponding discharge coefficient  $C_D$  (=0.333) that measured the ratio between the actual (computed here) discharge and the theoretical discharge is plotted, Figure 31, together with the measured points for various conditions and the agreement is in the range of uncertainty of the measurements.

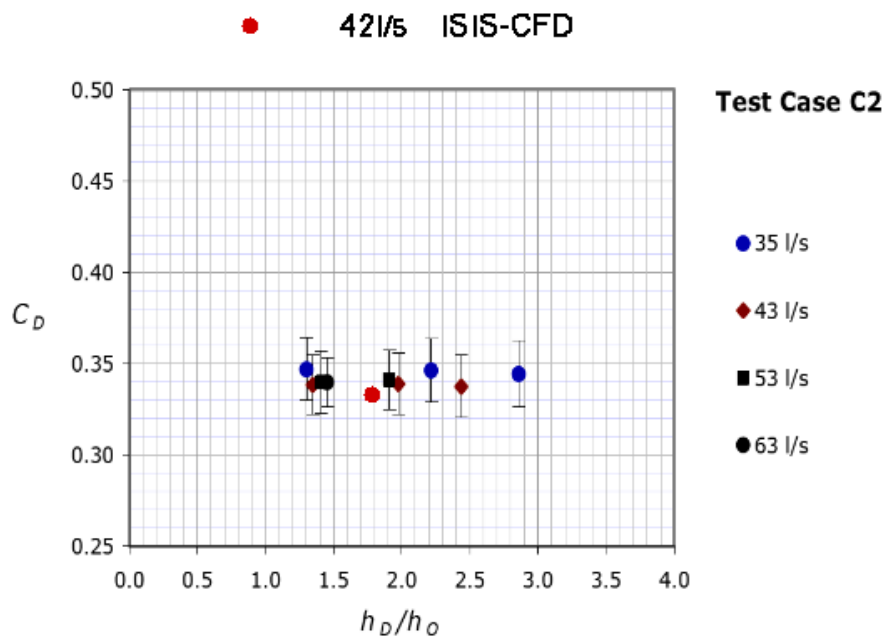


Figure 31 Plot of the discharge coefficient and the downstream head to opening height ratio: red filled circle for ISIS-CFD, other symbols for measurements.

### 3.4 Full scale simulations

The computational domain used in the previous section is simply scaled by a factor 3 corresponding to the scale factor of the model to obtain the full scale computational domain. The study was focused on two situations corresponding to two water heights at the inlet, keeping the same height at the outlet  $h_D=1.251\text{m}$ .

In a realistic situation, the cross-duct should be located typically 5m to 10m below the water level. In order to assess scale effects, a first water height of  $h_U=5\text{m}$  has been selected in order to match with the model scale simulation ( $h_U=1.67\text{m}$ ). A second study has been performed with an inlet water level  $h_U=10\text{m}$ .

Both full scale computations were performed similarly to the computation at model scale except the prescribed pressure values at inlet and outlet. For the full scale simulation, it was possible to increase the time step up to 0.03s without numerical instabilities once the flow was established (to be compared with the value of 0.001s used at model scale).

Figure 32 showing the instantaneous distribution of the axial velocity component in the middle Y cut has to be compared with Figure 29 for the model scale simulation (1.67m height at inlet). Except the maximum speeds, about 2m/s at model scale and 5.5m/s for the 10m full scale, the flow field develops similarly between the first and the last openings. The main difference occurs in the outlet box designed to prescribe the outlet pressure.

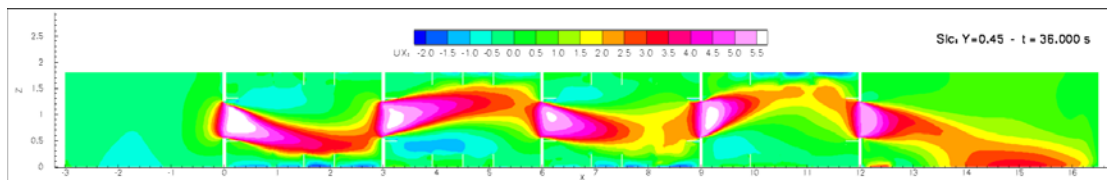


Figure 32 Axial velocity distribution in Y middle cut: 10m height at inlet

Concerning the turbulence modelling, Figure 33 for the turbulent viscosity distribution in the Y middle cut with 10m height at inlet, it is observed that in the inlet box designed to accommodate the prescribed pressure, a region of high mixing persists in the core of a large vortex. As shown from the plot of few streamlines in this cut, only part of the flow falling down from the inlet enters the first opening and the turbulence generated at the lower edge of the first opening feeds the recirculation where it remains. It follows that an improvement of the computational domain could be to reduce the extent of the inlet box but to extend the size of the outlet box.

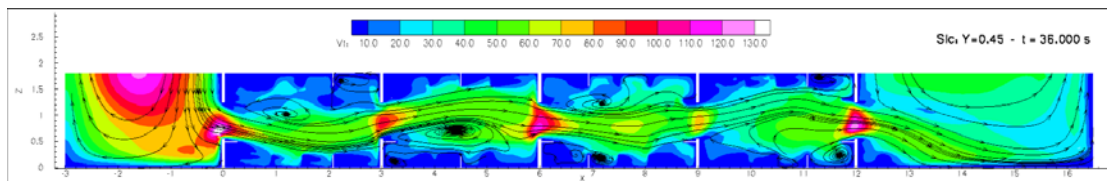


Figure 33 Turbulent viscosity distribution in Y middle cut: 10m height at inlet

With the 5m height at inlet, Figure 34, less turbulence is produced through each manhole with maximum turbulence levels divided by nearly a factor 2 compared to the 10m height situation. In the inlet box, the flow enters the first opening without generating a strong recirculation and the convection of the turbulence is reduced in that inlet box, contrary to the previous test case.

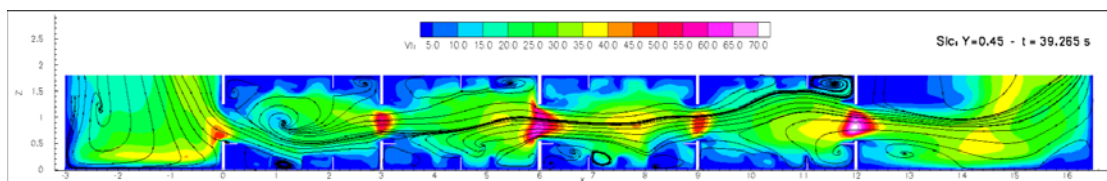


Figure 34 Turbulent viscosity distribution in Y middle cut: 5m height at inlet

The computed discharges and discharge coefficients are given in Table 4. Previous model scale result is also recalled as a reference. Both full scale computations were carried out at the same downstream head to opening height ratio  $h_D/h_0=1.782$ . It appears that both computed discharge coefficients for full scale simulations are similar within 3% and that the model scale coefficient is between these two full scale simulations with less than 2% of difference.

Case	Theoretical discharge (m <sup>3</sup> /s)	Computed discharge (m <sup>3</sup> /s)	Computed discharge coefficient
<i>Model scale</i>	<i>0.126</i>	<i>0.042</i>	<i>0.333</i>
Full scale, 5m	1.960	0.638	0.325
Full scale, 10m	3.140	1.051	0.335

*Table 4 Discharge and discharge coefficient for the two inlet water heights*

### 3.5 Conclusions

Both model and full scale simulations have been performed for the C2 submerged cross-duct. The geometry has been gridded with respect to the prescribed cross-duct geometry taking into account the presence of girders and stiffeners. The simulation with prescribed inlet and outlet water heights were made possible thanks to the use of prescribed pressure inlet and outlet boundary conditions.

The model scale flow was computed for a single point of discharge and the result concerning the discharge coefficient is in good agreement with the measurements.

The interest of CFD code is the possibility to simulate full scale simulations that cannot be reproduced experimentally. Two water heights at the inlet have been considered corresponding to real life situations. Both simulations predict a discharge coefficient in perfect agreement with the computed and experimental model scale. The trend of the full scale simulations indicates that no scale effect can be observed, at least for this unique downstream head to opening height ratio.

### 4. REFERENCES

1- "Pressure losses and flow velocities in flow through manholes and cross-ducts", Mikael Stening, Aalto University, D2.3 FLOODSTAND Deliverable, April 2010.

2- "An Interface Capturing Method for Free-Surface Hydrodynamic Flows", Patrick Queutey & Michel Visonneau, Computers & Fluids, Vol. 36, Issue 9, pp. 1481-1510, November 2007.